# A conductive scanning study of La0.67Sr0.33MnO3/Nb:SrTiO3 hetero-junction

H. X. Lu, J. Zhang, H. R. Zhang, Y. Li, Y. S. Chen, B. G. Shen, and J. R. Sun

Citation: Applied Physics Letters **108**, 051608 (2016); doi: 10.1063/1.4941419
View online: http://dx.doi.org/10.1063/1.4941419
View Table of Contents: http://scitation.aip.org/content/aip/journal/apl/108/5?ver=pdfcov
Published by the AIP Publishing



# A conductive scanning study of $La_{0.67}Sr_{0.33}MnO_3$/Nb:$SrTiO_3$ hetero-junction

H. X. Lu, J. Zhang, H. R. Zhang, Y. Li, Y. S. Chen,[a] B. G. Shen, and J. R. Sun[b]
*Beijing National Laboratory for Condensed Matter Physics and Institute of Physics, Chinese Academy of Sciences, Beijing 100190, People's Republic of China*

(Received 13 October 2015; accepted 25 January 2016; published online 4 February 2016)

Basing on conductive atomic force microscopy, we presented a direct conductance mapping for the interface of the $La_{0.67}Sr_{0.33}MnO_3$/Nb:$SrTiO_3$ hetero-junction. The most remarkable observation is the presence of an interfacial layer in Nb:$SrTiO_3$ adjacent to the manganite film. Within this layer, the AFM tip/Nb:$SrTiO_3$ contact shows a current-voltage dependence that strongly deviates from Shockley equation, unlike a Schottky diode. Spatial extension of this layer is explored and possible transport mechanism in or outside this interfacial layer is discussed. The present work gives a direct intuitional image on the interface of manganite junction. The principle proven here can be extended to other complex oxide interfaces. © *2016 AIP Publishing LLC*.
[http://dx.doi.org/10.1063/1.4941419]

Hetero-junctions are the simplest hetero-structures, exhibiting distinct properties characterized by electrical rectification and photoelectric effects. Compared with conventional semiconductor p-n junctions, complex oxide junctions are particularly interesting in a sense that they provide promising avenues towards powerful functionality that are highly desired by both fundamental and applied physics.[1] The most typical oxide junctions are formed by heavily hole-doped manganite and electron-doped $SrTiO_3$, which have been fabricated by Sugiura *et al.*[2] in 1999 and have been intensively studied since then, and versatile behaviors have been observed, such as rectifying transport,[1,2] photovoltaic effect,[3] magneto-resistance,[4–6] magneto-capacitance,[6,7] and interface polar-modulated rectification.[8,9]

As for conventional semiconductor p-n junctions, charge carrier exchange occurs between electron- and hole-doped oxides due to different Fermi levels, yielding an interfacial barrier. It is this barrier and its variation in external field that assigns manganite junctions distinct properties from the conventional ones. Obviously, the knowledge about interfacial state and the ability to tune this state are crucially important for a thorough understanding and an effective tuning of the emergent phenomena at oxide interfaces.

Fortunately, the semiconductor theory on the current-voltage (I-V) and capacitance-voltage (C-V) relations, which are originally proposed for conventional junctions, works well for manganite junctions, allowing a macroscopic characterization of this kind of junctions.[1] As revealed by an *in situ* photoelectron spectroscopy analysis,[8,10] a band bending develops in Nb:$SrTiO_3$ for the $La_{0.6}Sr_{0.4}MnO_3$/Nb:$SrTiO_3$ junction as the layer thickness of $La_{0.6}Sr_{0.4}MnO_3$ increases. This, as revealed by the quantitative analysis of the I-V and C-V relations, leads to an interfacial barrier of ~0.9 eV in height[8,11,12] and ~100 nm in width.[12] There are also indications for a slight variation of this barrier in magnetic fields,[5] yielding magnetically tunable junction resistance and photovoltaic effects.

We noticed that, despite of intensive studies in the past two decades, microscopic analyses on interfacial barrier are still very limited, such as the spatial distribution of the junction barrier and the effects of microstructure, which are important for an advanced exploration for emergent phenomena. Basing on the technique of conductive atomic force microscope (c-AFM), in this work we presented a conductive mapping of junction interface for $La_{0.67}Sr_{0.33}MnO_3$/Nb:$SrTiO_3$ (LSMO/NSTO). The most remarkable observation is the presence of an interfacial layer in NSTO adjacent to LSMO. Within this layer, the AFM tip/NSTO contact shows an I-V dependence that strongly deviates from Shockley equation, unexpected for an idea Schottky diode. The spatial extension of this layer is explored and its relation to depletion layer is discussed. The present work gives a conductive scanning study on depletion layer, which will be helpful for interface engineering of complex oxides.

Manganite junctions were prepared by depositing, via the pulsed laser (248 nm in wavelength) ablation technique, an LSMO film, ~200 nm in thickness, on a (001)-orientated 0.05 wt. % Nb-doped $SrTiO_3$ (NSTO) substrate ($5 \times 5 \times 0.5\,mm^3$). The fluence of the laser pulses was $1.5\,J\,cm^{-2}$, and the repetition rate was 2 Hz. The target-substrate separation was 4.5 cm. In the deposition process, the substrate temperature was kept at 700 °C and the oxygen pressure was fixed to 50 Pa. After deposition, the film was furnace-cooled to room temperature in an oxygen atmosphere of 200 Pa. The resulted sample was then cut into two pieces and pasted face to face, with its cross section being mechanically polished for AFM measurements. To remove possible contaminations resulted by mechanical polishing, the sample was ultrasonically cleaned in acetone, alcohol, and distilled water in sequence. The dried sample was transferred into the AFM chamber and heated to 150 °C for 30 min after pumping the chamber to $10^{-2}$ Torr to evaporate adsorbate. The whole system was then furnace-cooled to ambient temperature, and dry air was introduced into the chamber for subsequent measurements. For the c-AFM measurements, the bottom cross section of the junction was grounded by silver paste, and the local conductance was

[a]yschen@iphy.ac.cn
[b]jrsun@iphy.ac.cn

 

measured by a biased tip that swept through top cross section. A scanning probe microscopy (SPI 3800N, Seiko) was used for the conductive scanning study. A diamond-like carbon (DLC) tip which stands wear and tear was employed (with a diameter of ~30 nm). Two operation modes for the c-AFM measurements have been adopted, i.e., recording tip current while scanning a constantly biased tip through sample surface or recording the I-V characteristics while positioning tip at fixed locations. All experiments were conducted in dry air at ambient temperature.

Figure 1(a) is a schematic diagram of the experimental setup for AFM measurements. Fig. 1(b) exemplifies the topography of the cross section of LSMO/NSTO, and Fig. 1(c) is a simultaneously recorded current mapping, measured with a tip bias of 1 V. Despite the presence of mechanical scratches, the sample surface is fairly smooth. The root mean square roughness is ~10 nm, flat enough for the c-AFM measurements. From sample morphology, the LSMO/NSTO interface cannot be identified. This is understandable considering the similar mechanical properties of LSMO and NSTO. In contrast, the current mapping shows a sharp color contrast dividing the whole image into two parts. Since LSMO and DLC have similar work functions (~4.9 eV for LSMO[10] and ~5 eV for DLC), their contact should be Ohmic in nature. Therefore, tip currents are large above LSMO. The orientated dark lines may arise from mechanical defects appearing in the polishing process. For the DLC/NSTO contact, however, an interfacial barrier may be formed due to the low work function of NSTO (~3.9 eV), preventing electronic transport. According to the current mapping, the LSMO/NSTO interface is ~170 nm apart from the left edge of the topography (marked by a dashed line in Fig. 1(b)).

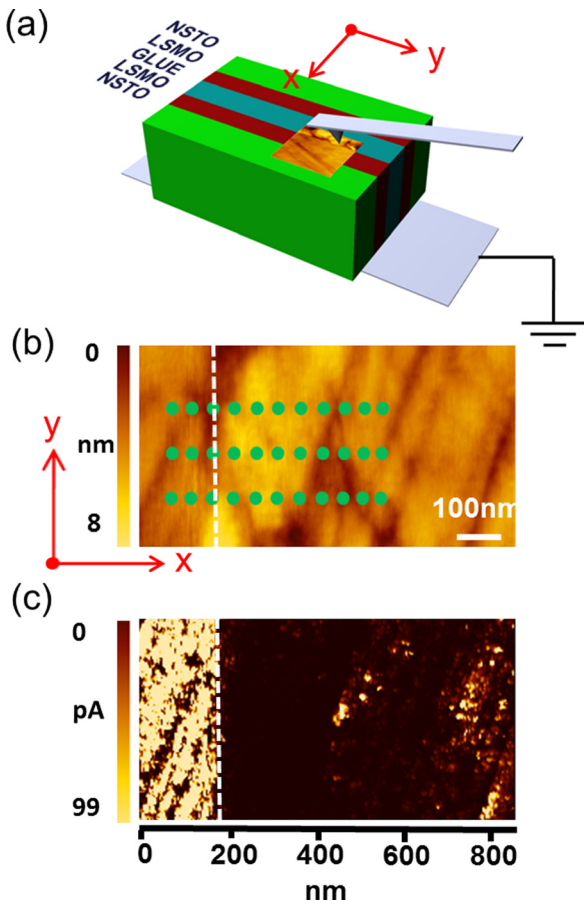


FIG. 1. (a) A schematic diagram for the experimental setup of conductive scanning measurements. Here a biased diamond-like carbon (DLC) tip was used. (b) Morphology of LSMO/NSTO the interface, showing a root mean square roughness of ~10 nm. Dashed line marks the interface between LSMO and NSTO. Spots mark the locations where the I-V characteristics were collected. (c) Current mapping on sample surface, measured under a tip bias of 1 V. All experiments were conducted in dry air, at ambient temperature.

One thing deserving special attention is the subtle difference in color contrast of the current image on NSTO. The image is dim on the left but slightly bright on the right. This result indicates that the surface conductivity is different in the near and far interface regions. In general, the color contrast of the current mapping is relatively low when recorded by rapid conductive scanning. To get a high spatial resolution, I-V curves were recorded by fixing AFM tip to different locations on the LSMO/NSTO interface. The tip was initially located at a point that is $x = 20$ nm apart from the left edge of the AFM image and shifted 10-nm farther after each measurement. Totally three set data were recorded, respectively, along three equally separated strips parallel to the $x$-axis of the specimen (marked by spot chains in Fig. 1(b)). As an example, in Figs. 2(a)–2(c), we show the I-V characteristics for one set data. Labels in the figures denote the $x$ coordinate of the AFM tip. All I-V curves collected on NSTO strongly deviate from linearity, indicating a non-Ohmic conduction. As discussed above, an interfacial barrier may be formed at the DLC/NSTO contact, affecting the charge transport processes. The most remarkable observation is the dramatic variation of the I-V dependence on tip location. Take the forward branch of the I-V curves as an example. In the near interface region, the tip current is negligibly small up to a bias voltage of 4 V. With the increase of tip distance, tip current emerges and rapidly develops into a jump to values exceeding the range of our c-AFM system (100 pA). This spatial dependence is a general feature of the I-V relations, also observed in other two set data. The conductance under reverse biases also shows a systematic variation with $x$, though it is relatively higher than that under forward biases.

Fixing tip bias to a constant value of 2 V and extracting the corresponding tip current from the I-V relations, we obtained the $I$-$x$ relations shown in Fig. 2(d). The tip current is very large for distant regions, beyond the capture of our c-AFM system (100 pA), and undergoes a steady decrease with the decrease of tip distance. Obviously, DLC/NSTO is a point contact. In case an electric bias is applied to the AFM tip, a radically distributed electric field, starting from the AFM tip and ending at back electrode, will be established. This will generate numerous paths for charge transport, along two paths AFM tip → NSTO and AFM tip → NSTO → LSMO. Since there are two energy barriers in the latter path (DLC/NSTO and LSMO/NSTO), the transport through AFM tip → NSTO could be dominant. Spatial variation of the conductance implies a change in field distribution in NSTO as AFM tip shifts. As will be discussed later, the band structure seen by the tip is different at different locations. Basing on the $I$-$x$ relations recorded from all three parallel strips, we obtained a current mapping on the $x$-$y$

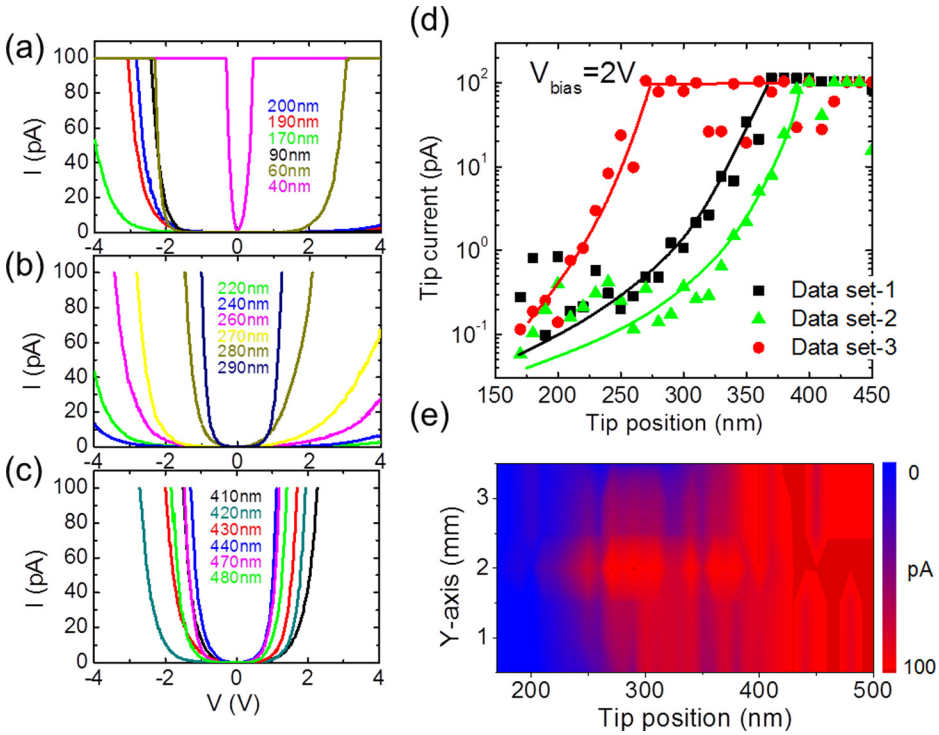


FIG. 2. (a)–(c) I-V characteristics of the DLC/NSTO contact, measured by positioning the AFM tip in different areas of the LSMO/NSTO interface. Labels in the figure mark the *x* coordinate of the AFM tip. (d) Spatial distribution of tip current, extracted from the I-V curves for a tip bias of 2 V. The upper limit of the tip current is 100 pA for our c-AFM system. Solid lines are guides for the eye. (e) A current mapping on the x-y plane, derived from the *I*-*x* relation presented in (d). All experiments were conducted in dry air, at ambient temperature.

plane shown in Fig. 2(e). Compared with Fig. 1(c), the color contrast of this figure is much higher, clearly demonstrating the spatial evolution of surface conductance of NSTO.

To get a clear idea on spatially dependent conduction, in Fig. 3(a) we present, in semi-logarithmic scale, a spatial dependence of the I-V curves along the *x*-axis (see supplementary material[13] for Figure S1). At first glance, the I-V curves incline as the AFM tip sweeps away from interface, signifying a variation in conductance. Remarkably, the ln(I)-V curves are strongly non-linear in the region close to interface, deviating from the thermionic emission process expected for an idea Schottky junction. It is possible that the interfacial NSTO has been influenced by adjacent LSMO, different from its interior. For distant regions, a linear ln(I)-V relation is observed, indicating a process following the Shockley equation. Adopting the Richardson parameter of 150 A cm$^{-2}$K$^{-2}$, an interface barrier between 0.60 and 0.65 eV and an ideality factor around ∼6 are deduced. The former is obviously lower than the difference of the work functions of DLC and NSTO (∼1 eV), and the latter is much greater than unity. Both phenomena imply the presence of interface states that may be introduced by mechanical

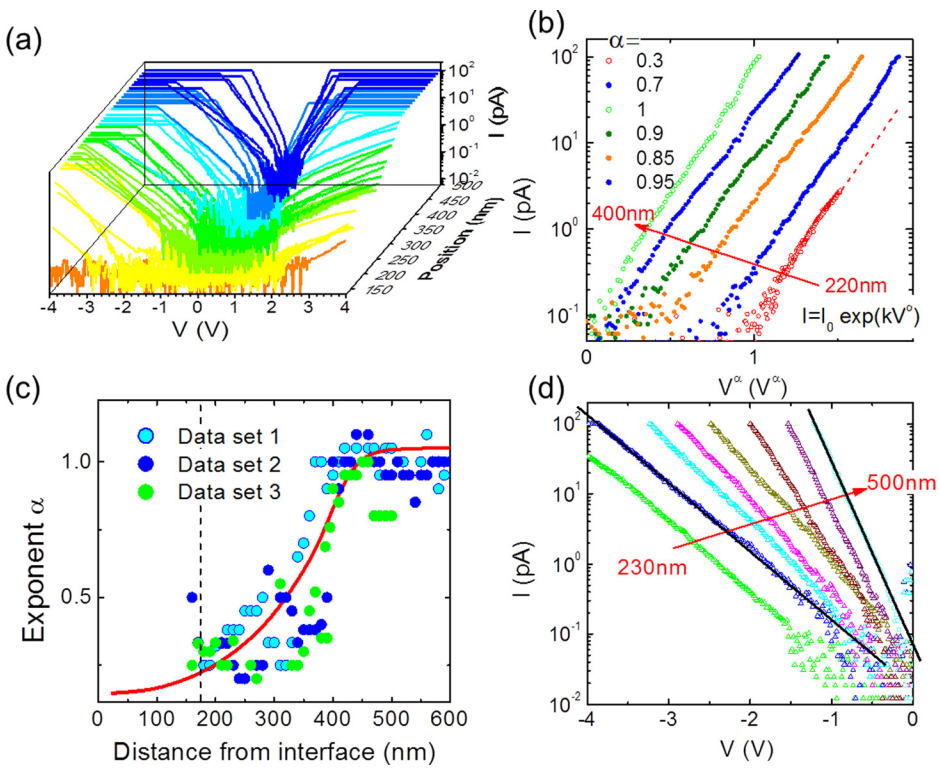


FIG. 3. (a) An expansion of the I-V characteristics along the *x*-axis, showing the spatial evolution of the transport behavior. (b) Forward branch of the I-V characteristics presented by replacing V with $V^{\alpha}$, where α is an exponent of position dependence. (c) Spatial distribution of the exponent α for three set data. Solid line is a guide for the eye. (d) Backward branch of the I-V characteristics. The fairly linear dependence of ln|I| on bias voltage implies (marked by straight lines) the occurrence of electron tunneling.

polishing. As will be seen later, interface states have a strong effect on transport process.

To gain further information on interfacial layer, we performed a quantitative analysis of the I-V curves and, fascinatingly, found a simple relation, $I = I_0 \exp(kV^{\alpha})$, for the forward branch of the I-V curves (Fig. 3(b)). (We have tried to analyze the I-V relation by the Shockley equation with a series resistance $R_S$[14] and found that the ln(I)–(V-IR$_S$) relation still obviously deviates from linearity) Although the underlying implications are not clear at present, the variation of $\alpha$ with $x$ allows a quantitative description of the interfacial layer.[15] As shown in Fig. 3(c), $\alpha$ is ~1 for distant regions and gradually reduces to ~0.25 towards interface. Defined by the sharp turn in the $\alpha$-$x$ curve, the layer thickness will be 230 nm (400 nm–170 nm). Corresponding to the decrease of $\alpha$, the ln(I)-V$^{\alpha}$ curve shows a right shift and the intercept on the I–axis exhibits a downward movement. These are apparent reasons for decreased conductance near interface.

Position-dependent transport behaviors were also observed under backward biases (Figs. 3(a) and 3(d)). Different from the typical Schottky junctions, the leakage current in reverse direction is sizable and varies strongly with bias voltage. The linear relation between ln|I| and |V| suggests electron tunneling through the DLC/NSTO contact (see supplementary material[13] for Figure S2).[16] As well established, interface states will depress the interfacial barrier, thus depletion layer width.[17] Sweeping AFM tip towards interface, the saturation current decreases, while the ln|I|-V slope fluctuates around ~1.5 ln(A)/V (see supplementary material[13] for Figure S3). As occurred under forward biases, the charge transport process is location-dependent, also becoming difficult near interface.

The spatially varied I-V characteristics cannot be ascribed to surface morphology, the latter is virtually homogeneous according to Fig. 1(b). The reduced conduction close to interface for NSTO implies the influence of LSMO on NSTO. As well known, LSMO and NSTO have different charge carriers. The former is heavily hole-doped (~$5.6 \times 10^{21}$ cm$^{-3}$), while the latter is electron-doped (~$4.3 \times 10^{18}$ cm$^{-3}$). When these two oxides meet each other, charge carrier exchange will take place because of different work functions (~4.9 eV for LSMO and ~3.9 eV for NSTO),[10] resulting in an interfacial barrier. I-V characteristic analysis shows that the LSMO/NSTO junction exhibits the typical diode behavior described by Shockley equation, and the deduced interfacial barrier is ~0.83 eV (see supplementary material[13] for Figure S4). Since the carrier concentration of NSTO is low, the depletion layer mainly appears in NSTO. In this layer, the conduction band edge ($E_C$) locates well above Fermi level ($E_F$) due to an upwards band bending (see supplementary material[13] for Figure S5). As a result, the energy band of the DLC/NSTO contact will be different in and outside the depletion layer. A schematic diagram for the band structure of the LSMO/NSTO junction is shown in Fig. 4(a), where $\Phi_B$ is the interfacial barrier, and $\Delta_1$ and $\Delta_2$ are the differences of $E_F$ and $E_C$ at locations "1" and "2," within and outside the depletion layer, respectively. Figs. 4(b) and 4(c) are two band diagrams formed when positioning AFM tip at "1" and "2," respectively. Here an ultrathin interfacial layer with a voltage drop of $\Delta$ has been proposed to

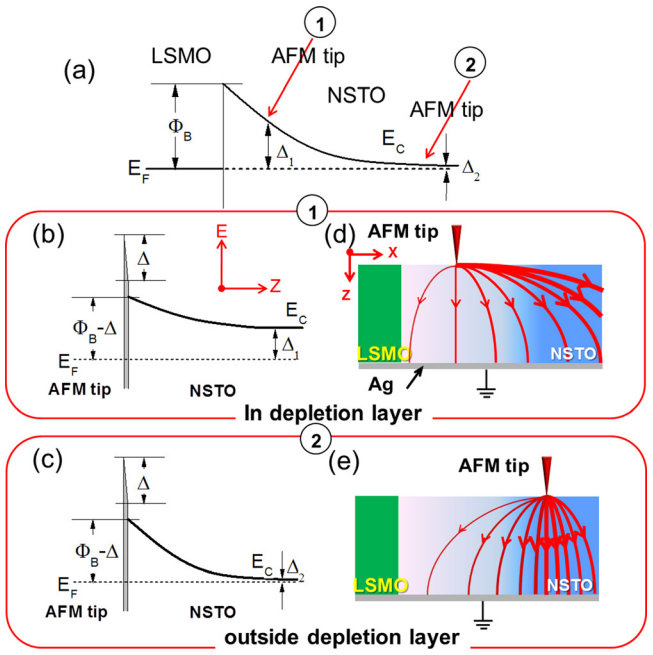


FIG. 4. (a) A schematic diagram for the band structure of the LSMO/NSTO junction, where $\Phi_B$ is interfacial barrier and $\Delta_1$ and $\Delta_2$ are the energy match between Fermi level ($E_F$) and conduction band edge of NSTO ($E_C$). Arrows mark the locations in and outside depletion layer. (b) and (c) Schematic band structures on the $E$-$z$ ($E$-$y$) plane for the DLC/NSTO contact in (b) and outside (c) the depletion layer. The large energy mismatch between $E_C$ and $E_F$ in (a) is obvious. (d) and (e) Schematic distribution of current density between AFM tip and back gate. It is more asymmetric when AFM tip locates in depletion region. Dense and thick lines mark high current densities.

accommodate interface states. Different from location "2," the conduction band of NSTO is much more flat at location "1." This difference will certainly influence the charge transport process. In general, the charge transport through the DLC/NSTO contact proceeds via two processes: thermionic emission over interfacial barrier and thermally assisted electron tunneling through interfacial barrier (shown by red and blue arrows in Figs. 4(b) and 4(c), respectively; also see supplementary material[13] for Figure S6). The former process could be similar in cases "1" and "2" because of the same barrier height, but the latter process is different; compared with case "2," in case "1" a much higher thermal energy is required for electron tunneling due to large $\Delta_1$. As a result, the surface conduction of location "1" is lower than that of location "2."

Finally, we will give a brief discussion on depletion width. According to the semiconductor theory, this layer thickness is ~$(2\varepsilon_0\varepsilon\Phi_B/eN_D)^{1/2} = 87$ nm, much narrower than that deduced from conductive scanning (~230 nm), where $e$ is the electron charge, $\varepsilon = 300$, is the dielectric constant of STO, $N_D = 4.3 \times 10^{18}$ cm$^{-3}$, is the carrier concentration of NSTO, and $\Phi_B = 1.1$ eV, is interfacial barrier. [Here the experimental value ~0.83 eV (see supplementary material[13] for Figure S4) was not used since the effect of thermally assisted electron tunneling, which always occurs in manganite junctions, will cause an underestimation of interfacial barrier] There are two reasons for this difference. First, since the current distribution between AFM tip and back electrode is radical, parts of the electric force lines may still penetrate through the depletion layer even when the AFM tip locates

well outside this layer, making the apparent layer thickness wide. Figs. 4(d) and 4(e) show the schematic distributions for current density between AFM tip and back electrode. The current lines are strongly asymmetric in case "1" and relatively symmetric in case "2." Thick lines represent high current density. Second, NSTO has been exposed to an oxygen pressure of 50 Pa at 700 °C for tens of minutes (which is required to thermally stabilize the temperature of the substrate) before depositing the LSMO film. This will introduce excessive oxygen into NSTO, causing a lower electron concentration in surface layer.

In summary, from the analysis of space-resolved I-V characteristics of the AFM tip/NSTO contact, firsthand information on the LSMO/NSTO interface is obtained. It is found that, due to carrier depletion, the near interface area of NSTO exhibits anomalous I-V dependences deviating from the Shockley equation which is expected for a typical AFM tip/NSTO contact. The spatial extension of this interfacial layer is explored and possible transport mechanism in and outside this layer is discussed. The present work gives a conductive mapping for junction interface, helpful for a thorough understanding of the unusual rectifying behaviors of manganite junctions.

This work has been supported by the National Basic Research of China (2013CB921701), the National Natural Science Foundation of China (11520101002, 11374348, 11134007, and 51590880), and the Key Program of the Chinese Academy of Sciences (KJZD-EW-M05).

[1]Y. Hikita and H. Y. Hwang, "Complex oxide Schottky junctions," in *Thin Films Metal-Oxides*, edited by S. Ramanathan (Springer, New York, 2010), Chap. 5.
[2]M. Sugiura, K. Uragou, M. Noda, M. Tachiki, and T. Kobayashi, Jpn. J. Appl. Phys., Part 1 **38**, 2675 (1999).
[3]J. R. Sun, C. M. Xiong, B. G. Shen, P. Y. Wang, and Y. X. Weng, Appl. Phys. Lett. **84**, 2611 (2004); Y. Hikita, M. Nishikawa, T. Yajima, and H. Y. Hwang, Phys. Rev. B **79**, 073101 (2009).
[4]H. Tanaka, J. Zhang, and T. Kawai, Phys. Rev. Lett. **88**, 027204 (2002); K. J. Jin, H. B. Lu, Q. L. Zhou, K. Zhao, B. L. Cheng, Z. H. Chen, Y. L. Zhou, and G. Z. Yang, Phys. Rev. **71**, 184428 (2005).
[5]W. M. Lü, J. R. Sun, Y. Z. Chen, D. S. Shang, and B. G. Shen, Appl. Phys. Lett. **95**, 232514 (2009).
[6]N. Nakagawa, M. Asai, Y. Mukunoki, T. Susaki, and H. Y. Hwang, Appl. Phys. Lett. **86**, 082504 (2005).
[7]B. T. Xie, Y. G. Zhao, and C. M. Xiong, Appl. Phys. Lett. **93**, 072112 (2008).
[8]M. Minohara, R. Yasuhara, H. Kumigashira, and M. Oshima, Phys. Rev. B **81**, 235322 (2010).
[9]T. Yajima, Y. Hikita, M. Minohara, C. Bell, J. A. Mundy, L. F. Kourkoutis, D. A. Muller, H. Kumigashira, M. Oshima, and H. Y. Hwang, Nat. Commun. **6**, 6759 (2015).
[10]M. Minohara, I. Ohkubo, H. Kumigashira, and M. Oshima, Appl. Phys. Lett. **90**, 132123 (2007).
[11]J. Matsuno, A. Sawa, M. Kawasaki, and Y. Tokura, Appl. Phys. Lett. **92**, 122104 (2008); M. Minohara, Y. Furukawa, R. Yasuhara, H. Kumigashira, and M. Oshima, Appl. Phys. Lett. **94**, 242106 (2009); F. A. Cuellar, G. Sanchez-Santolino, M. Varela, M. Clement, E. Iborra, Z. Sefrioui, J. Santamaria, and C. Leon, Phys. Rev. B **85**, 245122 (2012).
[12]K. G. Rana, S. Parui, and T. Banerjee, Phys. Rev. B **87**, 085116 (2013).
[13]See supplementary material at http://dx.doi.org/10.1063/1.4941419 for detailed information.
[14]F. Giannazzo, V. Raineria, S. Mirabella, G. Impellizzeri, and F. Priolo, Appl. Phys. Lett. **88**, 043117 (2006).
[15]In fact, different electronic processes which show different I-V dependences may occur simultaneously across the DLC/NSTO contact closing to the LSMO/NSTO interface, and the linear $\ln(I)$-$V^{\alpha}$ relation could be a phenomenological description of the total effects of these processes. In addition to the thermionic emission process for an ordinary Schottky junction [$\ln(I) \propto V$], the thermionic emission or Frenkel-Poole process across a metal-oxide-semiconductor (MOS) capacitor [$\ln(I) \propto V^{1/2}$] and the space-charge-limited process ($I \propto V^2$) are possible. When the relative contributions of these processes to I-V dependence change with tip position, $\alpha$ varies between 0.25 and 1.
[16]S. M. Sze and K. K. Ng, *Physics of Semiconductor Devices*, 3rd ed. (Wiley, New Jersey, 2007), pp. 227–229.
[17]S. M. Sze and K. K. Ng, *Physics of Semiconductor Devices*, 3rd ed. (Wiley, New Jersey, 2007), pp. 139–146.